Dynamical interferences as a probe of short-pulse-photoassociated rubidium dimers

Jordi Mur-Petit,* Eliane Luc-Koenig, and Françoise Masnou-Seeuws
CNRS Laboratoire Aimé Cotton, Univ. Paris-Sud, Bât. 505, F-91405 Orsay, France †
(Dated: December 15, 2006)

We analyze the formation of Rb_2 molecules with short photoassociation pulses applied to a cold ^{85}Rb sample. The laser field couples a continuum level of the ground electronic state $X^1\Sigma_g^+$ with bound levels in the $0_u^+(5S+5P_{1/2})$ and $0_u^+(5S+5P_{3/2})$ vibrational series. The non-adiabatic coupling between the two excited channels induces time-dependent beatings in the populations. We propose to take advantage of these oscillations either to probe the photoassociation process via a photoionization pulse, or to optimize the stabilization step into deep levels of the ground state.

PACS numbers: 32.80.Qk, 33.80.Ps, 34.50.Rk

Making ultracold molecules in the v=0 level of the ground electronic state is presently an important challenge since it opens the road toward coherent ultracold chemistry [1, 2]. Schemes based on photoassociation of ultracold atoms [3] with cw lasers, followed by radiative stabilization, have been very successful to form molecules in excited vibrational levels of the ground electronic state [4, 5]. The possibility of controlling the photoassociation reaction by use of short laser pulses has been discussed in theoretical papers [6, 7, 8] and very recently attempted by two experimental groups [9, 10], both in the rubidium case. The success of such experiments would create a bridge between the two domains of cold matter and coherent control, where femtosecond (fs) pulses are used to probe the dynamics of chemical reactions and to control the exit channels [11]. Up to now, photoassociation experiments with fs laser pulses have achieved *destruction* of the stable molecules already existing in the trap rather than creation of additional molecules. Indeed, whereas cw lasers red-detuned by 0.5-28 cm^{-1} relative to the D_2 line are efficient in populating levels in the external well of the $0_g^-(5S+5P_{3/2})$ potential [5], the scheme seems to be no longer working with broadband excitation [9, 10].

An alternative route is photoassociation with resonant coupling as realized in Cs_2 [12] and RbCs [13]. In the Rb_2 case, one populates the $0_u^+(5S+5P_{1/2})$ and $0_u^+(5S+5P_{3/2})$ coupled series. Several experimental and theoretical papers [14, 15, 16] have analyzed the strong perturbations in the Rb_2 vibrational spectra. The resonant coupling phenomenon has been proposed to optimize the stabilization step in pump-dump experiments [17]. However, one should first make sure that the levels populated in the photoassociation step do belong to the 0_u^+ series. The aim of the present paper is to propose a scheme for identifying $0_u^+(5S+5P_{1/2,3/2})$ molecules in short-pulse photoassociation experiments. We consider pulses in the picosecond range as they populate a limited number of bound vibrational levels. We show that characteristic time-dependent oscillations appear in photoionization probe signals or in the number of stabilized molecules.

Time-dependent fluorescence signals manifesting the coupling between the two series have been previously observed by pump-probe spectroscopy [18]. In this experiment, a molecular beam of Rb_2 is excited by a 120-fs laser pulse, from the $v = 0$ level of $X^1\Sigma_g^+$ to low vibrational levels of the $A^1\Sigma_u^+$ state, lying ~ 5600 cm^{-1} below the 5S+5P asymptote with a classical internal turning point around $8a_0$. A delayed pulse, operating in a suitable detection window around the outer turning point of the $b^3\Pi_u$ potential ($12a_0$), probes the population transferred to this state. It presents an oscillatory behavior with several characteristic periods of the order of 1 ps. This is explained in terms of interferences between several paths for the motion of the wavepacket in the excited state, due to the crossing of the $A^1\Sigma_u^+$ and $b^3\Pi_u$ potentials at $R_{\rm short} \approx 9.3a_0$. This crossing can be seen in Fig. 1(a), where we plot the potential energy curves corresponding to the two Hund's case a $A^1\Sigma_u^+$ and $b^3\Pi_u$ states [hereafter referred to as V_A and V_b], as determined by Bergeman *et al.* [19]. We also show the ground state potential obtained by matching *ab initio* calculations [20] to the long-range dispersion potential $-\sum_n C_n/R^n$ [21], and slightly shifting the repulsive barrier to reproduce the large value of the scattering length [22].

In this paper, we consider photoassociation at a moderate detuning of ≈ 60 cm^{-1} below the D_1 line, exciting loosely-bound vibrational levels of the coupled system in the vicinity of the up-to-now unexplored crossing at long range $R_{\rm long} \approx 29.2a_0$ [Fig. 1(c)]. Indeed, inclusion of the spin-orbit effective Hamiltonian H_{SO} lowers the energy of the b state by a quantity asymptoticaly ~ 79 cm^{-1}, giving rise to the diabatic curve $\bar{V}_b$, that crosses V_A at $R_{\rm long}$. The diagonalization of H_{SO} within the $\{A, \bar{b}\}$ subspace renders two Hund's case c $0_u^+(P_{1/2})$ and $0_u^+(P_{3/2})$ adiabatic curves, correlated to the $5S+5P_{1/2}$ and $5S+5P_{3/2}$ asymptotes, splitted by $\Delta E_{\rm fs} = 237$ cm^{-1}. The mixing angle $\theta(R)$ defines the transformation from the diabatic to the adiabatic basis at a given internuclear distance R:

$$|0_u^+(P_{1/2})\rangle = \cos\theta(R)\,|A\rangle + \sin\theta(R)\,|b\rangle\,, \quad (1a)$$

$$|0_u^+(P_{3/2})\rangle = -\sin\theta(R)\,|A\rangle + \cos\theta(R)\,|b\rangle\,. \quad (1b)$$

In the adiabatic representation, the two excited channels are coupled by radial coupling, which is governed

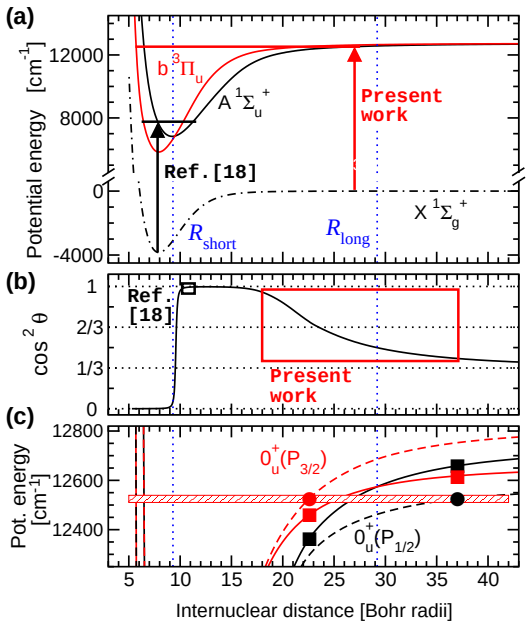

FIG. 1: (color online) (a) Potential energy curves for the ground state $X^1\Sigma_g^+$ (dash-dotted line), V_A (black, solid) and $\bar{V}_b$ (red, solid). (b) $|A\rangle$ component in $|0_u^+(P_{1/2})\rangle$ as given by Eqs. (1). (c) Zoom to the energy range where PA takes place, showing both diabatic (solid lines) and adiabatic (dashed) potentials. The shaded box indicates the PA window in the energy domain for the studied pulse. The dotted lines are at $R_{\rm short}$ and $R_{\rm long}$, and symbols stand for the classical turning points of the levels contributing to the decomposition of the excited wavepacket.

by the derivative $d\theta/dR$. We display in Fig. 1(b) the R-dependence of $\cos^2\theta$. There is a sharp variation, corresponding to a singlet-triplet change of character, in the region of $R_{\rm short}$ where the two diabatic curves cross abruptly. In the range of distances from 10 to 15 a_0, where the splitting between the diabatic curves is very large compared to $\Delta E_{\rm fs}$, the mixing angle becomes 0, so that $0_u^+(P_{1/2})$ has a pure singlet character. For $R > 15a_0$, $\cos^2\theta(R)$ decreases toward its asymptotic value 1/3, which, due to the very similar slopes of V_A and $\bar{V}_b$ at large R [cf. Fig. 1(c)], is only reached at distances far beyond $40a_0$. A complete mixing with $\theta = 45°$ occurs in the vicinity of $R_{\rm long}$. In contrast with the crossing at $R_{\rm short}$ explored in Ref. [18], this long-range crossing is not localized.

The system – We perform calculations for a system of ^{85}Rb atoms at a temperature of 100 μK as in usual photoassociation (PA) experiments [9, 10]. Only s-wave scattering and $J = 0$ rotational levels are considered. The three components of the radial wavefunction correspond to the electronic ground state ($X^1\Sigma_g^+ \equiv X$), and singlet ($A^1\Sigma_u^+ \equiv A$) and triplet excited states ($b^3\Pi_u \equiv b$). We introduce a Gaussian chirped pulse of energy $E_{\rm pulse}$, centered at time t_P, with a frequency that varies linearly,

$$\omega(t) = \omega_L + \chi \cdot (t - t_P)\,,$$

around the carrier frequency ω_L. The laser is red-detuned from the atomic D_1 line at ω_{D1} by $\Delta_L = \hbar(\omega_{D1} - \omega_L)$, χ is the linear chirp rate in the time domain, while the spectral bandwidth is $\delta\omega = 4\ln 2/\tau_L \approx 14.7\ {\rm cm}^{-1}/\tau_L$[in ps]. The instantaneous intensity of the pulse involves a Gaussian envelope

$$I(t) = \frac{E_{\rm pulse}}{\tau_C \sigma}\sqrt{\frac{4\ln 2}{\pi}}\exp\left[-4\ln 2\left(\frac{t-t_P}{\tau_C}\right)^2\right] \qquad (2)$$

with a FWHM equal to τ_C ($\geq \tau_L$), the pulse duration [23]. For this pulse, 98% of the energy $E_{\rm pulse}$ is delivered in the *time window* $[t_P - \tau_C, t_P + \tau_C]$ over the illuminated area σ [7]. During this time, the instantaneous laser frequency is resonant with all the excited levels with a binding energy in the range $[\Delta_L - \hbar|\chi|\tau_C, \Delta_L + \hbar|\chi|\tau_C]$, which defines a *photoassociation window in energy*. For the case of a single excited state, this can be translated into a *PA window in R* by the reflection principle [23].

We apply the rotating wave approximation on the instantaneous frequency to derive the dynamical equations [7, 8]. In our system, the laser couples the X state to the A excited channel, with a time dependent coupling $\hbar\Omega(t) = -\sqrt{I(t)/(2c\epsilon_0)}a(R)\mathcal{D}$, where c and ε_0 are the speed of light and permitivity of vacuum, $\mathcal{D} = 5.201$ a.u. is the relevant atomic electric-dipole moment (EDM) and $a(R)$ accounts for the R-dependence of the molecular EDM; at large distances $a(R) = \sqrt{2/3}$.

Numerical treatment – The low temperature of the experimental systems demands the use of a very large simulation box for the faithful inclusion as box-states of the continuum states above threshold [23]. To this end, a numerical grid up to $L = 30\,000a_0$ has been built with the Mapped Grid Method [24] and the dynamical equations have been time-propagated as in Ref. [7].

From now on, we concentrate on a short PA pulse that couples the scattering state $|X, E = 98.85\ \mu{\rm K}\rangle$ with levels $\approx 60\ {\rm cm}^{-1}$ below D_1 ($218\ {\rm cm}^{-1}$ below 5S+5P, corresponding to $\lambda_{\rm pump} = 798$ nm). The pulse is centered at $t_P = 50$ ps, with $\tau_C = 10$ ps, $\chi = 1.47\ {\rm cm}^{-1}\ {\rm ps}^{-1}$, and $E_{\rm pulse} = 41$ nJ focused on $\sigma = 2.8 \times 10^{-3}\ {\rm cm}^2$. We set the bandwidth to $\delta\omega \approx 15\ {\rm cm}^{-1}$ to avoid populating the dissociative levels in the excited states. The corresponding PA window in energy is indicated by the shaded box in Fig. 1(c).

Results – We present in Fig. 2 the free evolution of the wavepacket in the excited states, $\Psi_{\rm exc}(R,t)$, well after the PA pulse has finished. The photoassociation probability for a single pair of atoms is 4.21×10^{-6}, and most excited population concentrates around two peaks at $22a_0$ and $37a_0$. The relative importance of these peaks changes in time. For example, the peak at $22a_0$ that is present at $t = 72$ ps, has disappeared at $t = 76$ ps, but reappears at

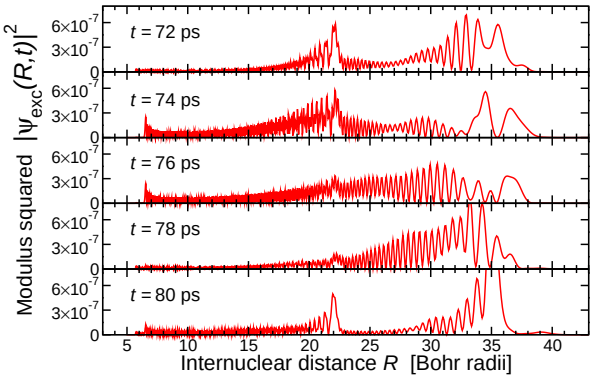

FIG. 2: (color online) Evolution of the wavepacket in the excited channels $\Psi_{\rm exc}(R,t)$ after the PA pulse has finished.

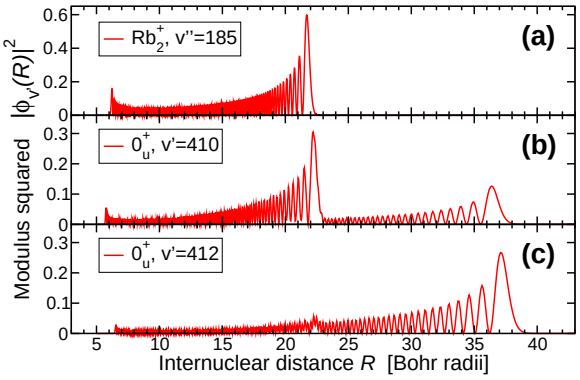

FIG. 3: (color online) Stationary wavefunctions of (a) the $Rb_2^+(X^2\Sigma_g^+)$ level bound by 264 cm^{-1}; (b) the 0_u^+ level 54 cm^{-1} below D_1; and (c) the 0_u^+ level 51 cm^{-1} below D_1.

$t = 80$ ps. Thus, a period $T_{\rm beat} \approx 8$ ps can be assigned to these oscillations.

This behavior can be understood in terms of quantum interferences between the various stationary levels that form the wavepacket. The excited wavepacket can be decomposed in the basis formed by the vibrational eigenfunctions $\phi_{v'}^{\rm coup}$ of the *coupled* 0_u^+ potentials, $\Psi_{\rm exc}(R,t) = \sum_{v'} c_{v'} \phi_{v'}^{\rm coup}(R) \exp[-iE_{v'}t/\hbar]$, where the summation is over the ~ 15 levels of energies $E_{v'}$ inside the PA window defined above. Each $c_{v'}$ as well as the total population in the excited potentials are constant after the pulse.

We show in Figs. 3(b) and (c) two $\phi_{v'}^{\rm coup}(R)$ wavefunctions present in the excited wavepacket under consideration. The wavefunction in the lower panel corresponds to a level 51 cm^{-1} below the $5S+5P_{1/2}$ limit. It turns out to be ascribeable to a "$0_u^+(P_{1/2})$ level", as most of its probability density is accumulated close to the outer turning point of this potential at this energy, $R_{\rm ext,\,1/2} \approx 37a_0$ [black circle in Fig. 1(c)]. More unusual is the wavefunction in panel (b), which corresponds to a level 54 cm^{-1} below $5S+5P_{1/2}$. This is a typical example of a "resonant $0_u^+(P_{3/2})$ level" [15]. It features two maxima of probability, corresponding to the turning points $R_{\rm ext,\,1/2}$ and $R_{\rm ext,\,3/2} \approx 22a_0$ [red circle in Fig. 1(c)] in $0_u^+(P_{1/2})$ and $0_u^+(P_{3/2})$ respectively. As the instantaneous frequency of the chirped pulse is resonant with ~ 15 levels in the coupled 0_u^+ series, the excited wavepacket will have components on stationary levels of both types, thus explaining the double-peak structure observed in Fig. 2.

Now, it is easy to show that the population density at an internuclear distance R has a time dependence determined by *all* the beating frequencies $\omega_{ij} = (E_i - E_j)/\hbar$, where E_i, E_j are the energies of those levels for which $c_{v'} \neq 0$. The largest weights in the decomposition correspond to $v' = 406$ and 408. These are two "$0_u^+(P_{1/2})$" levels separated by $\Delta E \approx 4.24$ cm^{-1}, which corresponds to a beating of 7.85 ps, in agreement with $T_{\rm beat}$.

One could also project the excited wavepacket on the uncoupled basis formed by the eigenstates of V_A and $\bar{V}_b$. In this case, many levels contribute, in particular, levels *outside* the energy PA window of the pulse. The largest contributions actually come from A and $\bar{\rm b}$ levels with classical turning points at $R_{\rm ext,1/2}$ and $R_{\rm ext,3/2}$, which correspond to the levels indicated by squares in Fig. 1(c). In fact, for the two strongly coupled A and $\bar{\rm b}$ states, a PA window cannot be defined in energy nor in R.

The observed beating in the population density close to a particular R can be probed experimentally with a suitable laser pulse that ionizes the molecule and coherently populates several levels of the lowest $Rb_2^+(X^2\Sigma_g^+)$ potential [25] with classical turning point $R_{\rm ext,\,+} \approx 22a_0$. The stationary wavefunction of one such level is plotted in Fig. 3(a). Assuming that the ionization process is a vertical transition, the population tranfer to the ionic channel will concern the part of the wavepacket that is close to $R_{\rm ext,+}$, *i.e.*, the peak around $R_{\rm ext,3/2}$. Indeed, we show in Fig. 4(a) the time evolution of the overlap $\sum_{v''} |\langle Rb_2^+(X^2\Sigma_g^+), v''|\Psi_{\rm exc}(t)\rangle|^2$ for the levels $v'' \in [185, 194]$ that have $R_{\rm ext,+} \approx 21 - 23a_0$ and can be populated using a laser with central wavelength $\lambda_{\rm probe} = 479.8$ nm and bandwidth $\delta\omega \approx 30$ cm^{-1}. The signal presents a rich structure of peaks and troughs. Nevertheless, the evolution is dominated by three timescales, roughly $T_1 \approx 15$ ps, $T_2 \approx 4.5$ ps and $T_3 \approx 28$ ps. These times correspond to the beatings between the levels $v' = 407$ and 408 [two "$0_u^+(P_{1/2})$" levels] for T_1, $v' = 406$ and 410 [the first one being "$0_u^+(P_{1/2})$" while $v' = 410$ is a "resonant $0_u^+(P_{3/2})$" level, cf. Fig. 3(b)] for T_2, and for T_3 both $v' = 405$-406 and $v' = 409$-410 [both being "$0_u^+(P_{1/2})$-$0_u^+(P_{3/2})$" beatings]. Quite remarkably, a similar ionizing pulse designed to probe the wavepacket close to $37a_0$ ($\lambda_{\rm probe} = 469.3$ nm) would render a signal where only T_1 appears [cf. Fig. 4(b)]: as the classical turning point of the $0_u^+(P_{3/2})$ components is $22a_0 \ll 37a_0$, almost no effect of the $0_u^+(P_{1/2})$-$0_u^+(P_{3/2})$ coupling is expected to show up at this distance.

We have finally analyzed the dynamics after a dump

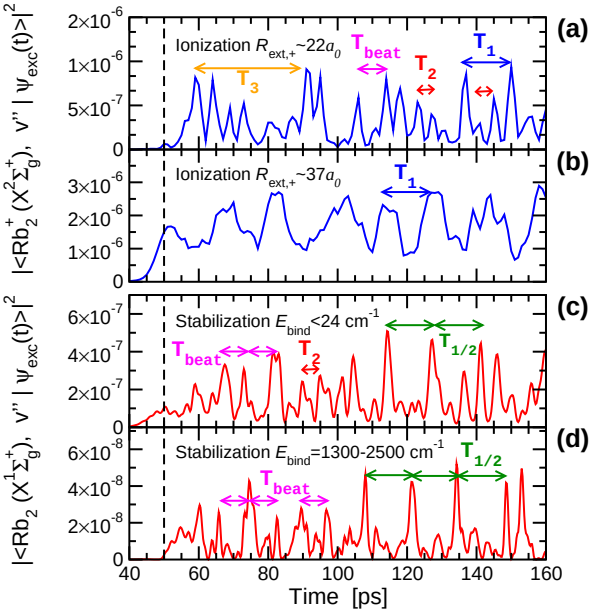

FIG. 4: (color online) Evolution of the overlap of $|\Psi_{\rm exc}(t)\rangle$ with (a) 10 $Rb_2^+(X^2\Sigma_g^+)$ levels with $R_{\rm ext} \approx 22a_0$; (b) 16 $Rb_2^+(X^2\Sigma_g^+)$ levels with $R_{\rm ext} \approx 37a_0$; (c) 17 $Rb_2(X^1\Sigma_g^+)$ levels with $E_{\rm bind} \lesssim 24$ cm^{-1}; (d) 28 $Rb_2(X^1\Sigma_g^+)$ levels with $E_{\rm bind} \approx 1300 - 2500$ cm^{-1}. The vertical line stands for $t_P = 50$ ps and arrows indicate the most relevant timescales.

pulse toward bound vibrational levels of the electronic ground state, $Rb_2(X^1\Sigma_g^+)$. The results are shown in Fig. 4(c) for the vibrational levels with binding energy $E_{\rm bind} \lesssim 24$ cm^{-1}, and in Fig. 4(d) for the levels with 1300 cm^{-1} $\leq E_{\rm bind} \leq$ 2500 cm^{-1}, which have a reasonable Franck-Condon factor with $|\Psi_{\rm exc}(t)\rangle$. In both cases, the mean value of the vibrational period in the pure $0_u^+(P_{1/2})$ potential at this energy, $T_{1/2} \approx 13$ ps, has an important role. (The stabilization is more efficient toward the higher-lying levels as the corresponding outer turning points are in the range $[R_{\rm ext,3/2}, R_{\rm ext,1/2}]$.)

In summary, we have studied the dynamics of Rb_2 0_u^+ molecules created by a picosecond PA pulse from a cold sample of ^{85}Rb atoms. The excited wavepacket spans $\sim$ 15 vibrational levels in the coupled 0_u^+ basis and presents two maxima of probability at $R_{\rm ext,\,1/2}$ and $R_{\rm ext,\,3/2}$. The subsequent dynamics shows quantum intereferences, with a beating of the population close to $R_{\rm ext,\,3/2}$. We have argued that this beating can be monitored by photoionizing the wavepacket with a laser with well-defined energy spectrum which, in practice, defines a window of internuclear distances whose density probability is probed. We have also analyzed the time-dependence in a pump-dump sequence to form bound ground-state molecules. Fourier analysis of these oscillations has been performed, showing a complex pattern of frequencies that will be published elsewhere. In the future, we will further study the role of SO coupling in ^{87}Rb and ^{133}Cs samples and with fs PA pulses using a mask to avoid dissociation.

We thank T. Bergeman, M. Aymar and S. Azizi for providing us the data of the potentials in Refs. [19] and [20, 25], respectively. Fruitful discussions with C. Koch, E. Dimova, O. Dulieu, R. Kosloff, A. Montmayrant, L. Pruvost, I. Walmsley and M. Weidemüller are also gratefully acknowledged. This work was partially supported by the EC RTN "Cold Molecules" (contract no. HPRN-CT-2002-00290).

* Electronic address: jordi.mur@lac.u-psud.fr
† Laboratoire Aimé Cotton is UPR 3321 of CNRS associée à l'Université Paris-Sud, member of the Fédération Lumière Matière (LUMAT FR 2764) and of the Institut Francilien de Recherche sur les Atomes Froids (IFRAF).

[1] D. J. Heinzen, R. Wynar, P. D. Drummond, and K. V. Kheruntsyan, Phys. Rev. Lett **84**, 5029 (2000).
[2] N. Balakrishnan and A. Dalgarno, Chem. Phys. Lett. **341**, 652 (2001).
[3] K. M. Jones, E. Tiesinga, P. D. Lett, and P. S. Julienne, Rev. Mod. Phys. **78**, 483 (2006).
[4] A. Fioretti *et al.*, Phys. Rev. Lett. **80**, 4402 (1998).
[5] C. Gabbanini *et al.*, Phys. Rev. Lett. **84**, 2814 (2000).
[6] J. Vala *et al.*, Phys. Rev. A **63**, 013412 (2001).
[7] E. Luc-Koenig, R. Kosloff, F. Masnou-Seeuws, and M. Vatasescu, Phys. Rev. A **70**, 033414 (2004).
[8] C. P. Koch, E. Luc-Koenig, and F. Masnou-Seeuws, Phys. Rev. A **73**, 033408 (2006).
[9] B. L. Brown, A. J. Dicks, and I. A. Walmsley, Phys. Rev. Lett. **96**, 173002 (2006).
[10] W. Salzmann *et al.*, Phys. Rev. A **73**, 023414 (2006).
[11] H. Rabitz, R. de Vivie-Riedle, M. Motzkus, and K. Kompa, Science **288**, 824 (2000).
[12] C. M. Dion *et al.*, Phys. Rev. Lett. **86**, 2253 (2001).
[13] A. J. Kerman *et al.*, Phys. Rev. Lett. **92**, 153001 (2004).
[14] C. Amiot, O. Dulieu, and J. Vergès, Phys. Rev. Lett. **83**, 2316 (1999).
[15] V. Kokoouline, O. Dulieu, and F. Masnou-Seeuws, Phys. Rev. A **62**, 022504 (2000).
[16] H. Jelassi, B. V. de Lesegno, and L. Pruvost, Phys. Rev. A **74**, 012510 (2006).
[17] C. P. Koch, R. Kosloff, and F. Masnou-Seeuws, Phys. Rev. A **73**, 043409 (2006).
[18] B. Zhang, N. Gador, and T. Hansson, Phys. Rev. Lett. **91**, 173006 (2003).
[19] T. Bergeman *et al.*, J. Phys. B: Atom. Mol. Opt. Phys. **39**, S813 (2006).
[20] M. Aymar and O. Dulieu (2006), private communication.
[21] A. Marte *et al.*, Phys. Rev. Lett. **89**, 283202 (2002).
[22] E. G. M. van Kempen, S. J. J. M. F. Kokkelmans, D. J. Heinzen, and B. J. Verhaar, Phys. Rev. Lett. **88**, 093201 (2002).
[23] E. Luc-Koenig, M. Vatasescu, and F. Masnou-Seeuws, Eur. Phys. J. D **31**, 239 (2004).
[24] K. Willner, O. Dulieu, and F. Masnou-Seeuws, J. Chem. Phys. **120**, 548 (2004).
[25] M. Aymar, S. Azizi, and O. Dulieu, J. Phys. B: Atom. Mol. Opt. Phys. **36**, 4799 (2003).